Self-Templated Synthesis of Nanoporous CdS Nanostructures for Highly Efficient Photocatalytic Hydrogen Production under Visible Light

Ningzhong Bao,*,† Liming Shen,† Tsuyoshi Takata, and Kazunari Domen

Department of Chemical System Engineering, School of Engineering, The University of Tokyo, 7-3-1 Hongo, Bunkyo-Ku, Tokyo 113-8656, Japan

Received October 11, 2007. Revised Manuscript Received November 5, 2007

Nanoporous CdS nanostructures, including nanosheets and hollow nanorods, have been prepared by a two-step aqueous route, which consists of a first precipitation of nanoporous $Cd(OH)_2$ intermediates and a subsequent S^{2-}/OH^- ion-exchange conversion of the obtained $Cd(OH)_2$ used as template either to nanoporous CdS nanosheets with sizes up to 60 nm and an average thickness of about 9 nm or to CdS hollow nanorods with lengths up to 30 nm and outer diameters in the range 7–14 nm. The obtained CdS nanostructures containing nanopores with diameters of ~3 nm exhibit a very large BET surface area of about 112.8 $m^2\ g^{-1}$. A very high hydrogen yield of about 4.1 mmol h^{-1} under visible light irradiation ($\lambda \geq 420$ nm), corresponding to the highest apparent quantum yield of about 60.34% measured at 420 nm so far reported, has been attained over the obtained nanoporous CdS nanostructures loaded with monodisperse 3–5 nm Pt nanocrystals, which is due to an efficient charge separation, a fast transport of the photogenerated carriers, and a fast photochemical reaction at the CdS/electrolyte interface. The photocatalytic reaction conditions, such as the Pt-loading content, the amount of catalyst, and the concentration of sacrificial regents, have been optimized.

1. Introduction

Hydrogen, an attractive sustainable clean energy source, is currently obtained from nonrenewable natural gas, petroleum, and coal but could in principle be generated from the renewable resource of water.[1–7] The photosplitting of water is an attractive environmental-friendly method, which offers a way of capturing available solar energy and converting it into valuable hydrogen.[8–11] However, most of developed photocatalysts capable of splitting water are mixed transition metal oxides with wide band gaps, which can only take advantage of ultraviolet irradiation constituting only 4% of the incoming solar energy. Considerable efforts have been focused on developing visible-light-driven photocatalysts, such as limited mixed oxides,[12–14] (oxy)nitrides,[15–21] and (oxy)sulfdes,[22,23] capable of using the less energetic but more abundant visible light ($\lambda \geq 420$ nm) accounting for about 43% of the solar spectrum.

Sulfides, such as CdS, $ZnS-CuInS_2$ solid solution, etc., have narrow band gaps and valence bands at relatively negative potentials, which offer them good visible-light-driven photocatalytic activities in the presence of sacrificial reagents.[24–32] The usage of sacrificial reagents, such as S^{2-},

* Corresponding author: Tel 205-348-5041; fax 205-348-9104; e-mail nzhbao@mint.ua.edu.

† Present address: Center for Materials for Information Technology (MINT), The University of Alabama, Tuscaloosa, AL 35487.

(1) Maeda, K.; Teramura, K.; Lu, D.; Saito, N.; Inoue, Y.; Domen, K. *Angew. Chem., Int. Ed.* **2006**, *45*, 7806.
(2) Maeda, K.; Teramura, K.; Lu, D.; Takata, T.; Saito, N.; Inoue, Y.; Domen, K. *Nature (London)* **2006**, *440*, 295.
(3) Ishikawa, A.; Takata, T.; Kondo, J. N.; Hara, M.; Kobayashi, H.; Domen, K. *J. Am. Chem. Soc.* **2002**, *124*, 13547.
(4) Kim, H. G.; Borse, P. H.; Choi, W.; Lee, J. S. *Angew. Chem., Int. Ed.* **2005**, *44*, 4585.
(5) Zou, Z.; Ye, J.; Sayama, K.; Arkawa, H. *Nature (London)* **2001**, *414*, 625.
(6) Gratzel, M. *Nature (London)* **2001**, *414*, 338.
(7) Khan, S. U. M.; Al-shahry, M.; Ingler, W. B., Jr *Science* **2002**, *279*, 2243.
(8) Bard, A. J.; Fox, M. A. *Acc. Chem. Res.* **1995**, *28*, 141.
(9) Khaselev, O.; Turner, J. A. *Science* **1998**, *280*, 425.
(10) Fujishima, A.; Honda, K. *Nature (London)* **1972**, *238*, 37.
(11) Kato, H.; Asakura, K.; Kudo, A. *J. Am. Chem. Soc.* **2003**, *125*, 3082.
(12) Kudo, A.; Omori, K.; Kato, H. *J. Am. Chem. Soc.* **1999**, *121*, 11459.
(13) Kato, H.; Kudo, A. J. *Phys. Chem. B* **2001**, *105*, 4285.
(14) Kato, H.; Kudo, A. *J. Phys. Chem. B* **2002**, *106*, 5029.
(15) Chun, W.; Ishikawa, A.; Fujisawa, H.; Takata, T.; Kondo, J. N.; Hara, M.; Kawai, M.; Matsumoto, Y.; Domen, K. *J. Phys. Chem. B* **2003**, *107*, 1798.
(16) Kasahara, A.; Nukumizu, K.; Takata, T.; Kondo, J. N.; Hara, M.; Kobayashi, H.; Domen, K. *J. Phys. Chem. B* **2003**, *107*, 791.
(17) Hara, M.; Chiba, E.; Ishikawa, A.; Takata, T.; Kondo, J. N.; Domen, K. *J. Phys. Chem. B* **2003**, *107*, 13441.
(18) Maeda, K.; Takata, T.; Hara, M.; Saito, N.; Inoue, Y.; Kobayashi, H.; Domen, K. *J. Am. Chem. Soc.* **2005**, *127*, 8286.
(19) Maeda, K.; Teramura, K.; Lu, D.; Saito, N.; Inoue, Y.; Domen, K. *Angew. Chem., Int. Ed.* **2006**, *45*, 7806.
(20) Lee, Y.; Terashima, H.; Shimodaira, Y.; Teramura, K.; Hara, M.; Kobayashi, H.; Domen, K.; Yashima, M. *J. Phys. Chem. C* **2007**, *111*, 1042.
(21) Ito, S.; Thampi, K. R.; Comte, P.; Liska, P.; Gratzel, M. *Chem. Commun.* **2005**, 268.
(22) Ishikawa, A.; Yamada, Y.; Takata, T.; Kondo, J. N.; Hara, M.; Kobayashi, H.; Domen, K. *Chem. Mater.* **2003**, *15*, 4442.
(23) Ishikawa, A.; Takata, T.; Matsumura, T.; Kondo, J. N.; Hara, M.; Kobayashi, H.; Domen, K. *J. Phys. Chem. B* **2004**, *108*, 2637.
(24) Tsuji, I.; Kato, H.; Kobayashi, H.; Kudo, A. *J. Am. Chem. Soc.* **2004**, *126*, 13406.
(25) Tsuji, I.; Kato, H.; Kudo, A. *Angew. Chem., Int. Ed.* **2005**, *44*, 3565.
(26) Tsuji, I.; Kato, H.; Kudo, A. *Chem. Mater.* **2006**, *18*, 1969.
(27) Tsuji, I.; Kato, H.; Kobayashi, H.; Kudo, A. *J. Phys. Chem. B* **2005**, *109*, 7323.

10.1021/cm7029344 CCC: $40.75
Published on Web 12/06/2007

SO_3^{2-}, etc., prevents sulfide photocatalysts from the anodic photocorrosion by providing sacrificial electron donors to consume the photogenerated holes. At the same time, it promotes hydrogen evolution through making up half of the water-splitting reaction.[33–35] Because the extraction products, such as sulfides, sulfites, etc., of fossil energy resources now being produced in large quantities are undesirable and polluting byproduct in hydrogenation and flue-gas desulfurization processes at chemical plants, the photocatalytic reaction yielding valuable hydrogen energy over sulfides from aqueous solution containing S^{2-} and SO_3^{2-} is very attractive both for achieving practical photocatalytic hydrogen production using sunlight and in solving the environmental problem caused by the petrochemical industries.

The CdS photocatalysts with good photocatalyic activity process the combination of materials-related characteristics in particularly requiring hexagonal crystal structure, good crystallinity, large surface area, good dispersity, short bulk-to-surface diffusion distance for e^- and h^+, and monodisperse cocatalyst−sulfide surface nanostructures, which contributes to an efficient charge separation, a fast transport of the photogenerated carriers, and a fast photochemical reaction at the photocatalyst/electrolyte interface.[36–38] The Ag_2S-activated ZnS-doped colloidal CdS nanocrystals are the most active CdS ever reported, exhibiting a very high quantum yield of 37% at 450 nm, which is due to a very large surface area of >100 m^2 g^{-1}.[35] However, it suffers from disadvantages of serious particle agglomeration and unstability. Compared with the above Ag_2S-activated ZnS-doped colloidal CdS nanocrystals, a relatively higher quantum yield of 25% at 450 nm has been achieved over platinized pure CdS powder which is stable but has a low specific surface area of <6.7 m^2 g^{-1}. Therefore, there is large room for a further improvement of the photocatalytic activity of pure CdS by increasing the surface area.[39]

Nanoporous sheetlike/hollow CdS nanostructures can be prepared in relatively large sizes up to dozens of nanometers, which decreases the particle agglomeration occurring in many colloidal nanocrystals. Meanwhile, at least the thickness of the sheetlike nanostructures or the wall of hollow nanostructures has the size down to several nanometers. Electrons and holes generated inside the CdS are able to quickly migrate to the surface of CdS, passing a shorter distance of either half of the thickness or near to the nanopore wall, which greatly decreases the bulk e^-/h^+ recombination. At the same time, a quick surface e^-/h^+ separation, a fast interfacial charge carrier transfer, and an easy charge carrier trapping are achieved, which is due to the factor that the large surface area and the nanoporous structure ensure the strong abilities to interact with ions, atoms, and molecules not only on the outer surface but also throughout the whole nanostructures.[40–44] As a result, the nanoporous sheetlike/hollow CdS nanostructures are capable of exhibiting highly visible-light-driven photocatalytic activity for hydrogen production.[45–47] On the other hand, there still exist several disadvantages for the nanoporous/hollow nanostructures. First, the synthesis of materials containing nanopores and hollow structures often requires synthetic templates, and thus a simple, direct, and low-cost synthesis approach needs to be developed.[40] Second, microporous solids, such as zeolites, etc., consist of three-dimensional crystalline frameworks and interpenetrating small micropore channels (<1 nm in diameter), which cannot allow the fixation of large molecules, the reduction of the diffusion restriction of reactants, reactions involving bulky molecules, and in particular for the aqueous heterogeneous photocatalytic reaction involving sacrificial reagents.[48–50] Third, the majority of mesoporous (2–50 nm diameter) materials, in particular for nonoxides, cannot be synthesized in crystalline form, and only several limited semicrystalline mesoporous materials have been reported.[51–53] Therefore, the development of a simple, mild, and effective synthetic method to directly prepare crystalline nanoporous CdS nanostructures is a key step for achieving highly efficient photocatalytic hydrogen production under visible light.

In this study, we report a simple, aqueous solution route for the large-scale preparation of crystalline nanoporous CdS nanostructures at room temperature under air condition using air-insensitive inorganic reactants of $CdCl_2 \cdot 2.5H_2O$ and $Na_2S \cdot 9H_2O$. The synthesis procedure involves an initial precipitation of nanoporous $Cd(OH)_2$ nanosheets and nanorods in aqueous solution and a subsequent S^{2-}/OH^- ion-exchange conversion of the obtained $Cd(OH)_2$ intermediates to CdS. The obtained CdS nanostructures loaded with monodisperse uniform Pt nanocrystals exhibit the highest apparent quantum yield of about 60.34% at 420 nm for photocatalytic hydrogen production in the presence of sacrificial reagents of Na_2SO_3 and Na_2S, showing the potential for practical photocatalytic hydrogen production

(28) Shangguan, W.; Yoshida, A. *J. Phys. Chem. B* **2002**, *106*, 12227.
(29) Fujishiro, Y.; Uchida, S.; Sato, T. *Int. J. Inorg. Mater.* **1999**, *1*, 67.
(30) Lei, Z.; Ma, G.; Liu, M.; You, W.; Yan, H.; Wu, G.; Takata, T.; Hara, M.; Domen, K.; Li, C. *J. Catal.* **2006**, *237*, 322.
(31) Tricot, Y. M.; Fendler, J. H. *J. Am. Chem. Soc.* **1984**, *106*, 2475.
(32) Uchihara, T.; Matsumura, M.; Yamamoto, A.; Tsubomura, H. *J. Phys. Chem.* **1989**, *93*, 5870.
(33) Bulher, N.; Meier, K.; Reber, J. F. *J. Phys. Chem.* **1984**, *88*, 3261.
(34) Reber, J. F.; Meier, K. *J. Phys. Chem.* **1984**, *88*, 5903.
(35) Reber, J. F.; Rusek, M. *J. Phys. Chem.* **1986**, *90*, 824.
(36) Kudo, A.; Kato, H.; Tsuji, I. *Chem. Lett.* **2004**, *33*, 1534.
(37) Fox, M. A.; Dulay, M. T. *Chem. Rev.* **1995**, *83*, 341.
(38) Bao, N.; Shen, L.; Takata, T.; Domen, K.; Gupta, A.; Yanagisawa, K.; Grimes, A. C. *J. Phys. Chem. C*, **2007**, *111*, 17527.
(39) Matsumura, M.; Furukawa, S.; Saho, Y.; Tsubomura, H. *J. Phys. Chem.* **1985**, *89*, 1329.
(40) Davis, M. E. *Nature (London)* **2002**, *417*, 813.
(41) Bao, N.; Shen, L.; Yanagisawa, K. *J. Phys. Chem. B* **2004**, *108*, 16739.
(42) Bao, N.; Feng, X.; Yang, Z.; Shen, L.; Lu, X. *Environ. Sci. Technol.* **2004**, *38*, 2729.
(43) Lu, D.; Hitoki, G.; Katou, E.; Kondo, J. N.; Hara, M.; Domen, K. *Chem. Mater.* **2004**, *16*, 1603.
(44) Ito, S.; Thampi, K. R.; Comte, P.; Liska, P.; Gratzel, M. *Chem. Commun.* **2005**, 268.
(45) Bao, N.; Shen, L.; Takata, T.; Lu, D.; Domen, K. *Chem. Lett.* **2006**, *35*, 318.
(46) Zheng, N.; Bu, X.; Vu, H.; Feng, P. *Angew. Chem., Int. Ed.* **2005**, *44*, 5299.
(47) Hu, J.; Ren, L.; Guo, Y.; Liang, H.; Cao, A.; Wan, L.; Bai, C. *Angew. Chem., Int. Ed.* **2005**, *44*, 1269.
(48) Corma, A. *Chem. Rev.* **1997**, *97*, 2373.
(49) Soler-Illia, G. J.; de, A. A.; Sanchez, C.; Lebeau, B.; Patarin, J. *Chem. Rev.* **2002**, *102*, 4093.
(50) Ying, J. Y.; Mehnert, C. P.; Wong, M. S. *Angew. Chem., Int. Ed.* **1999**, *38*, 56.
(51) Katou, T.; Lee, B.; Lu, D.; Kondo, J. N.; Hara, M.; Domen, K. *Angew. Chem., Int. Ed.* **2003**, *42*, 2382.
(52) Yang, P.; Zhao, D.; Margolese, D. I.; Chmelka, B. F.; Stucky, G. D. *Nature (London)* **1998**, *396*, 152.
(53) Crepaldi, E. L.; Soler-Illia, G. J.; de, A. A.; Grosso, D.; Cagnol, F.; Ribot, F.; Sanchez, C. *J. Am. Chem. Soc.* **2003**, *125*, 9970.

using sunlight. The present synthesis strategy could be a general method for other binary sulfides.

2. Experimental Section

2.1. Preparation and Characterization of Photocatalysts. In a typical synthesis, the white $Cd(OH)_2$ intermediate was precipitated by adding 10 mL of 0.1 M $CdCl_2 \cdot 2.5H_2O$ aqueous solution to 100 mL of 0.1 M NaOH aqueous solution under stirring for 2 min at room temperature. The obtained white $Cd(OH)_2$ intermediate was then converted to yellow CdS by adding 10 mL of 0.1 M $Na_2S \cdot 9H_2O$ to the above solution under continuous stirring for 5 min. The obtained CdS precipitate was collected, washed with distilled water for several times, and finally dried overnight in an oven at 70 °C. The obtained CdS were investigated using a combination of characterization technologies including N_2 Sorption (BEL, BELsorp-mini), transmission electron microscopy (TEM, coupled with high-resolution (HR) and energy dispersive spectroscopy (EDS), Tecnai F-20), scanning electron microscopy (Hitachi S-4700), X-ray diffraction (XRD, Rigaku RINT-UltimaIII; Cu Kα), and ultraviolet–visible diffuse reflectance spectra (UV–vis DRS, JASCO V-560).

2.2. Photocatalytic Reaction. Photocatalytic reactions were carried out in a closed gas circulation and evacuation system fitted with a top window Pyrex cell. Prior to the photocatalytic reaction, the CdS powders were uniformly platinized by a 0.5 h photoreduction of 1 wt % H_2PtCl_6 with UV light irradiated using a 450 W high-pressure Hg lamp. Approximately 0.15 g of Pt-loaded CdS photocatalyst was dispersed by a magnetic stirrer in 200 mL of aqueous solution containing 0.35 M Na_2SO_3 and 0.25 M Na_2S as sacrificial reagents. The photocatalysts were irradiated with visible light ($\lambda \geq 420$ nm) using a cutoff filter from a 300 W Xe lamp. The temperature of the reactant solution was maintained at room temperature by providing a flow of cooling water during the photocatalytic reaction. The amount of hydrogen evolved was determined with online gas chromatography.

The apparent quantum yield was measured under the same photocatalytic reaction except for the wavelength of irradiation light. The hydrogen yields of 10 h photocatalytic reaction in one continuous reaction under visible light with different wavelengths of 420, 470, 500, 520, 560, and 600 nm were measured. Apparent quantum yields at different wavelengths were calculated by the following function. The band-pass and cutoff filters and a photodiode were used in measurement.

$$\text{apparent} = \frac{\text{number of photons used to generate } H_2}{\text{total number of photons under irradiation at fixed wavelength}}$$

Photocatalytic hydrogen production by irradiating suspensions containing platinized CdS and the electrolytes of S^{2-} and SO_3^{2-} has shown very high efficiency. The addition of SO_3^{2-} can efficiently suppress the formation of disulfide (S_2^{2-}) ions, allowing hydrogen to evolve at a high rate. Chemical analysis has been used to confirm the photodegradation products of sacrificial regents of S^{2-} and SO_3^{2-}. SO_4^{2-} ions in the presence of SO_3^{2-} and $S_2O_3^{2-}$ ions were analyzed by precipitation with $BaCl_2$ solution. The excess of $BaCl_2$ was then titrated with EDTA solution. After SO_3^{2-} ions were separated by flushing N_2 through the acidified solution, the concentration of S_2^{2-} ions was determined by oxidation with a hot solution of $K_2Cr_2O_7$. Analysis of $S_2O_3^{2-}$ ions in the presence of S^{2-} and SO_3^{2-} ions was carried out iodometrically after separating S^{2-} ions by precipitation with zinc acetate in an alkane medium and masking SO_3^{2-} with formaldehyde.

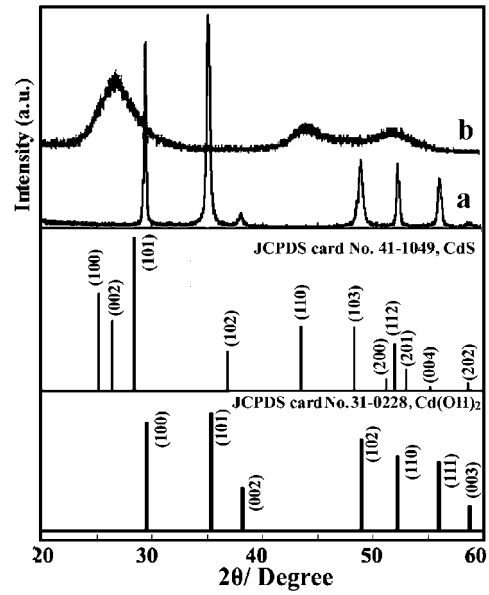

Figure 1. XRD patterns of (a) $Cd(OH)_2$ intermediates and (b) as-made hexagonal CdS and standard XRD patterns of $Cd(OH)_2$ (JCPDS No. 31-0228) and hexagonal CdS (JCPDS No. 41-1049).

3. Results and Discussion

3.1. Characterizations and Properties of Photocatalysts. XRD patterns of the $Cd(OH)_2$ intermediates and the CdS products, together with the standard diffraction patterns of $Cd(OH)_2$ and hexagonal CdS, are depicted in Figure 1. All the different peaks of products are well indexed either as the $Cd(OH)_2$ (JCPDS card No. 31-0228) in Figure 1a or as the hexagonal CdS (JCPDS card No. 41-1049) in Figure 1b. Figure 1b shows three very broadening diffraction peaks attributed to the (002), (110), and (112) planes of a hexagonal phase of CdS. The average grain sizes, calculated from the full width at half-maximum (fwhm, in radians), of the (101) line for the $Cd(OH)_2$ intermediates and the (101) line for the CdS products using the Scherrer formula are 12.4 and 3.5 nm, respectively.

The morphology, structure, and composition of the obtained products have been investigated by TEM, HRTEM, SEM, and EDS. The $Cd(OH)_2$ intermediates (Figure 1) are composed of nanosheets of dozens of nanometers in size and nanorods of 9–14 nm in diameter and 40–60 nm in length. The HRTEM image (Figure 2a2) of a typical individual $Cd(OH)_2$ nanosheet shows clear crystal lattices with short-range continuous size up to 5 nm, indicating the polycrystalline nature of the nanosheets. HRTEM image (Figure 2a3) of a typical individual nanorod clearly shows large-scale continuous crystal lattices with an interplanar distance of about 0.3 nm corresponding to the (100) plane, confirming the single crystalline nature of the nanorods. Nanopores with diameter of ~3 nm are observed within both nanosheets and nanorods.

The $Cd(OH)_2$ intermediates have been converted to CdS via a S^{2-} ion-exchange reaction. As shown in Figure 2b1, the shape and size of the obtained CdS nanostructures are very close to those of the $Cd(OH)_2$ intermediates. A HRTEM

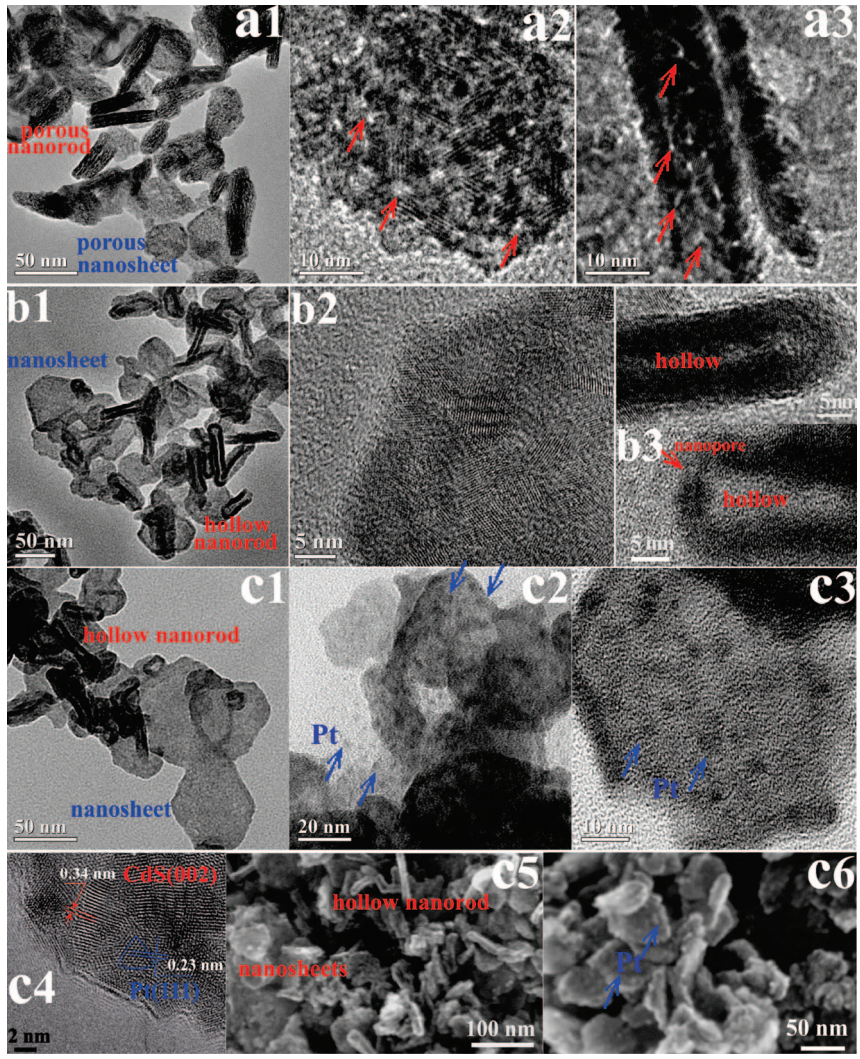

Figure 2. TEM, HRTEM, and SEM images of the products formed at various synthetic steps. (a1−a3) TEM images of $Cd(OH)_2$ intermediates: (a1) TEM image of typical $Cd(OH)_2$ intermediates; (a2) and (a3) respectively are TEM images of an individual nanosheet and nanorod both containing nanopores marked with red arrows. (b1−b3) TEM and HRTEM images of nanoporous nanosheets and hollow nanorods of polycrystalline CdS: (b1) TEM image of typical CdS nanostructures; (b2) and (b3) respectively are HRTEM images of individual nanosheet and hollow nanorod of polycrystalline CdS. (c1−c6) TEM, HRTEM, and SEM images of Pt-loaded CdS nanosheets and hollow nanorods: (c1) TEM image of typical Pt-loaded CdS nanostructures; (c2, c3) magnified TEM images of CdS nanosheets showing monodisperse Pt nanocrystals on the surface; (c4) HRTEM image of an individual Pt-loaded CdS nanosheet, showing crystal lattices of both CdS and Pt; (c5, c6) SEM images of Pt-loaded CdS nanostructures. Some Pt nanocrystals have been marked with blue arrows in parts c1, c2, and c6.

image (Figure 2b2) of an individual CdS nanosheet shows many random arranged crystal lattices with short-range continuous sizes, which indicates a polycrystalline nature of the CdS nanosheets. Figure 2b3 shows HRTEM image of two CdS hollow nanorods with inner diameters of 2.8 and 6.2 nm. Both of the CdS hollow nanorods have clear, continuous crystal lattices, indicating the single crystalline nature of the obtained hollow CdS nanorods. A penetrable nanopore, marked with a red arrow in Figure 2b3, is observed at one end of a hollow nanorod. The obtained CdS nanostructures with special nanopores and hollow structures have never been reported.

Pt nanocrystals have been uniformly photodeposited on the obtained CdS nanostructures. No morphologic and structural differences have been observed between the as-made CdS nanostructures (Figure 2b1) and the Pt-loaded CdS nanostructures (Figure 2c1). The EDS spectra (not shown) of the Pt-loaded nanoporous CdS nanostructures show strong Cd and S signals with Cd:S ratios of 1:1.03, which indicates the $Cd(OH)_2$ intermediates have been totally converted to CdS. Furthermore, Pt signal with 8% content (the atom content to Cd) was also detected. As shown in Figure 2c2,c3, monodisperse Pt nanocrystals with uniform size of about 3 nm have been deposited on the surface of CdS nanostructures. HRTEM image (Figure 2c4) of a CdS nanosheet shows two different clear crystal lattices with interplanar distances of 0.34 nm of the CdS(002) plane and 0.23 nm of the Pt(111) plane. More stereomicrographs of the Pt-loaded CdS nanostructures were obtained using SEM. As shown in Figure 2c5, either nanosheets with size up to 50 nm and thickness of around 9 nm or the hollow nanorods with diameter of around 10 nm and length up to 40 nm were observed in the CdS products covering with monodisperse Pt nanocrystals (see Figure 2c6), in good agreement with the above TEM results.

Textural property of the obtained nanoporous CdS nanostructures has been determined by N_2 adsorption/desorption isotherms and corresponding pore size distribution. As shown

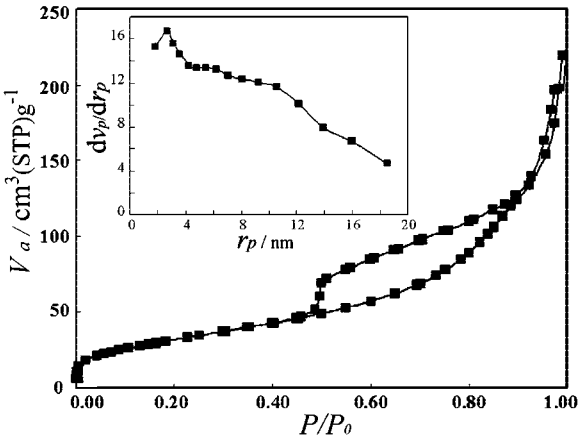

Figure 3. Nitrogen adsorption/desorption isotherms and pore diameter distribution (the inset, calculated from the adsorption branch using the BJH method) of as-made CdS nanostructures.

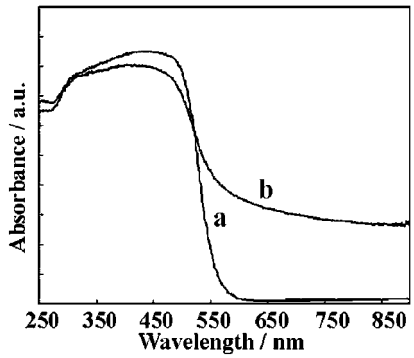

Figure 4. UV–vis diffuse reflectance spectrum of (a) as-made hexagonal CdS and (b) 10 wt % Pt-loaded CdS nanostructures.

in Figure 3, two well-defined steps at P/P_0 of 0.5–0.9 and 0.9–1 were observed on the N_2 adsorption/desorption isotherms. The former gives a typical type IV isotherm with a clear H1-type hysteresis loop which is characteristic of mesoporous materials. The latter of the uptake at high pressure is associated with the empty spaces between nanoparticles. A relatively narrow pore size distribution with maximum at around 3.3 nm is also shown in the inset of Figure 3, in agreement with the TEM results. Other typical textural parameters of the as-made CdS nanostructures are BET surface area of 112.8 $m^2\ g^{-1}$ and pore volume of 0.38 $cm^3\ g^{-1}$, which are very high for crystalline semiconductor sulfides.

Figure 4 show the UV–vis diffuse reflectance spectra of the as-made CdS and the Pt-loaded CdS nanostructures, corresponding to a band gap of about 2.25 eV, which are comparable to the measured value for the standard bulk CdS sample (about 2.4 eV). Generally, there exist critical sizes on nanoscale for semiconductors exhibiting a blue shift in the absorption spectrum. As for the CdS, a blue shift can be observed in the absorption spectrum when the size of CdS is smaller than 5 nm.[54,55]Although the structural units of the present CdS nanostructures have a relatively fine size of about 5 nm, the macroscopic size of each individual

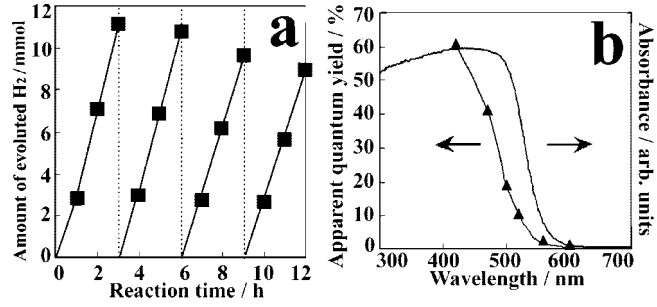

Figure 5. (a) Time course of hydrogen yield over 0.15 g of Pt-loaded CdS ($\lambda \geq 420$ nm) from an aqueous solution containing 0.25 M Na_2SO_3 and 0.35 M Na_2S under visible-light irradiation, four runs in one continuous reaction. (b) Influence of wavelength on the apparent quantum yield for hydrogen production over 0.15 g of Pt-loaded CdS from fresh aqueous solution containing 0.25 M Na_2SO_3 and 0.35 M Na_2S under visible-light irradiation with various wavelengths of 420, 470, 500, 520, 560, and 600 nm.

nanostructure is larger than decades of nanometers, which could be the reason why the absorption spectrum does not exhibit a blue shift.

3.2. Photocatalytic Activity of Nanoporous CdS Nanostructures. Figure 5a shows the photocatalytic activity of the Pt-loaded CdS nanostructures decreased slightly after four run reactions in one continuous reaction. The initially photocatalytic hydrogen yield attained 4.1 mmol h^{-1}. After the fourth reaction runs, the photocatalyst retained 80% of the initial photocatalytic activity under visible light irradiation and reached a stable hydrogen yield of 3.1 mmol h^{-1}. Figure 5b shows an action spectrum for hydrogen evolution from an aqueous solution containing both 0.35 M Na_2SO_3 and 0.25 M Na_2S over the Pt(10 wt %)-loaded photocatalysts of CdS nanostructures. The onset of the action spectrum agrees well with that of the diffuse reflection spectrum. Hydrogen evolution stopped by absorption in the tail region (>600 nm), revealing that the visible-light response of the photocatalyst is due to the band-gap transition between the valence and conduction bands. The quantum yield of the Pt-loaded CdS nanostructures is 60.34% at 420 nm, which is the highest apparent quantum yield so far reported. Previous results reported active Ag_2S activated CdS doping with ZnS showing a high quantum yield of 37% at 450 nm, but the materials are less stable than platinized pure CdS powders, giving a quantum yield of 25% at 450 nm at 60 °C.[32,33] The apparent quantum yield decreased with increasing the active wavelength until the lowest value of about 0.2% at 600 nm. Hydrogen evolution did not appear by absorption in the region of >600 nm because only photons of a wavelength shorter than 600 nm can induce photochemical reactions. The change tredency of the quantum yields at different waverlengths should agree with that of the UV–vis DSR.[24,33] The quantum yield at 450 nm should be close to that obtained at 420 nm because of the agreeable absorbance at both 420 and 450 nm. The present results show that the quantum yield at 450 nm is about 20% lower than 60.34% at 420 nm, which is due to the fact that, in the present study, we measured the quantum yields at 420, 470, 500, 520, 560, and 600 nm in one continuous reaction, and the reaction at each wavelength continued for 10 h, which caused the decreased hydrogen evolution rate because of both the contamination of the platinum oxidized at the CdS surface by sulfurous products to form platinum sulfide and an increasing concentration of

(54) Nakanishi, T.; Ohtani, B.; Uosaki, K. *J. Phys. Chem. B* **1998**, *102*, 1571.
(55) Wang, Y.; Suna, A.; Mahler, W.; Kosowski, R. *J. Chem. Phys.* **1987**, *87*, 7315.

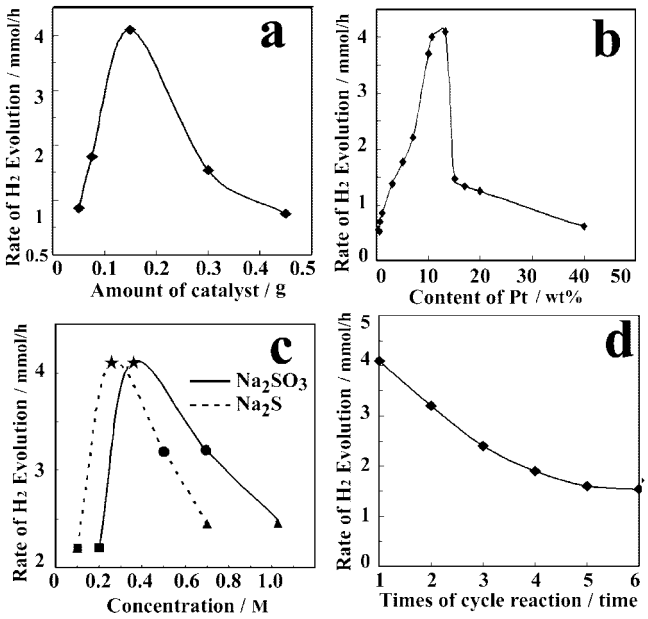

Figure 6. (a) Relation of the amount of CdS catalyst loaded with 10 wt % Pt nanocrystals to the hydrogen evolution rate from an aqueous solution containing 0.25 M Na_2SO_3 and 0.35 M Na_2S. (b) Relation of the Pt-loading content to the hydrogen evolution rate from an aqueous solution containing 0.25 M Na_2SO_3, 0.35 M Na_2S, and 0.15 g of CdS catalyst. (c) Relation of the concentration of sacrificial regents to the hydrogen evolution rate from an aqueous solution containing 0.15 g of Pt-loaded CdS and sacrificial regents of Na_2S and Na_2SO_3 at different concentrations. (d) Hydrogen evolution rates from aqueous solutions containing 0.25 M Na_2SO_3, 0.35 M Na_2S, and 0.15 g of 10 wt % Pt-loaded CdS catalyst for each of the six 12 h reations. All reactions were performed under visible-light irradiation provided by a light source, 300 W Xe lamp with a cutoff filter (λ > 420 nm).

the oxidation state of sacrificial regents suppressing the proceeding of photocatalytic reaction.

Optimized photocatalytic conditions for the highest hydrogen yield have been investigated, considering the factors such as the amount of photocatalyst, the content of loaded Pt nanocrystals, and the concentration of sacrificial regents. Figure 6a shows the influence of the amount of photocatalysts on the rate of hydrogen evolution. The rate of hydrogen evolution rapidly increases from 0.85 mmol h^{-1} in the presence of 0.05 g of Pt-loaded CdS to the maximum rate of 4.1 mmol h^{-1} in the presence of 0.15 g of Pt-loaded CdS and then decreases to 0.75 mmol h^{-1} in the presence of 0.45 g of Pt-loaded CdS. The hydrogen production rate stably increases as the photons are continuously injected into the semiconductors. The usage ratio of all the photons from the irradiation in photocatalytic reaction containing diluted photocatalysts is low because a lot of photons either pass through the solution without being absorbed by the photocatalysts or are reflected by the glass reactor wall. With increasing the concentration of photocatalysts, the number of photons absorbed by the photocatalysts increases and the number of photons reflected by the glass reactor decreases. The total amount of the photons absorbed by the photocatalysts thus increases. As the concentration of photocatalysts reached a critical value at which the photons absorbed by the photocatalysts reached the stable maximum, however, the photons cannot be continuously injected into photocatalyst particles, which increases the recombination of electrons and holes. Therefore, the hydrogen production rate decreases again. All in all, the reason is due to the combination effect of thermodynamic and kinetic factors of the photoelectron generation and transfer in heterogeneous photocatalytic reactions. An optimal amount of photocatalysts is required in order to attain the highest photocatalytic efficiency. In the present study, the optimal amount of photocatalysts is smaller than those of previous reported data because the present CdS nanostructures have relatively fine particle size, nanoporous structure, and much larger surface area.[32,33] Both bulk and surface electron/hole pairs quickly separate and migrate to the CdS−electrolyte interface via a much shorter distance, reducing water to hydrogen and oxidizing the sacrificial reagents.

Figure 6b shows the dependence of the rate of hydrogen evolution upon the amount of Pt cocatalyst loaded on the CdS photocatalyst. The photocatalytic activity of the pure CdS photocatalyst was as low as 0.02 mmol h^{-1} and unstable but was greatly improved after loading with Pt nanocrystals. As shown in Figure 6b, the hydrogen yield rapidly increases from 0.55 mmol h^{-1} at a 0.5% Pt loading to the maximum rate of 4.1 mmol h^{-1} at a 13% Pt loading. However, with continuously increasing the Pt loading content, the hydrogen yield quickly decreases to 1.4 mmol h^{-1} at 15% Pt loading and then slowly decreases to 0.62 mmol h^{-1} at 40% Pt loading, which is due to a shielding effect of the Pt cocatalyst. We also observed that the as-made Pt-loaded CdS photocatalyst becomes much darker with increasing the Pt-loading concentration, which is because of the increasing surface Pt coverage. The presence of metal particles, particularly Pt, on the surface of the CdS microcrystals drastically decreases the luminescence intensity. This expected quenching action of Pt indicates that Pt particles are very efficient traps for electrons.[56]

Figure 6c shows the influence of the concentration of sacrificial regents of Na_2SO_3 and Na_2S. H_2O is reduced to hydrogen by the electrons photogenerated in the conduction band accompanied by oxidation of sacrificial reagents. There exists an optimal concentration of 0.35 M for Na_2SO_3 and 0.25 M for Na_2S for the maximal hydrogen evolution rate. Generally, concentrated sacrificial reagents could be expected for the better diffusion of the reacting species to the surface of photoatalysts. On the other hand, as the pH increases under basic conditions, the negative shift has been observed for both the flat-band potential of CdS and the redox potential of H^+/H_2. However, the flat-band potential of CdS becomes less negative than the redox potential of H^+/H_2, leading to a decrease in the reactivity of the CdS photocatalyst in the present of sacrificial regents, such as SO_3^{2-}, formic acid, formaldehyde, methanol, etc.[57,58] Further, the flat-band potential of CdS also depends on the concentration of S^{2-}.[34] With increasing the concentration of S^{2-}, the flat-band potential of CdS located more negative than the redox potential of H^+/H_2. However, the S_2^{2-} ions, forming from the oxidation of S^{2-} ions, have a less negative reduction potential than photons, which results in a decreasing ef-

(56) Hengleln, A.; Llndlg, B.; Westerhausen, J. *J. Phys. Chem.* **1981**, *85*, 1627.
(57) Matsumura, M.; Hiramoto, M.; Irhara, T.; Tsubomura, H. *J. Phys. Chem.* **1984**, *88*, 248.
(58) Matsumura, M.; Saho, Y.; Tsubomura, H. *J. Phys. Chem.* **1984**, *88*, 3807.

ficiency of hydrogen production. Moreover, hydrogen evolution would become thermodynamically difficult in a strongly alkaline medium. In the present study, the reaction solution is basic because of the hydrolysis of SO_3^{2-} and S^{2-}ions. The decrease of the rate of hydrogen production in highly alkaline conditions, caused by the hydrolysis of concentrated SO_3^{2-} and S^{2-}, is explained by the relation among the energy level of the conduction band of CdS, the redox potential of H^+/H_2, the concentration of S^{2-}, and the pH value of solutions described above. Therefore, the highest hydrogen evolution rate cannot be attained in the presence of either diluted or concentrated sacrificial reagents.

Since photocatalysts for solar energy conversion need a long-term stability, the rate of hydrogen evolution during a longer period of illumination has been examined. Figure 6d shows the rate of H_2 evolution from solutions containing 0.25 M Na_2SO_3, 0.35 M Na_2S, and 0.15 g of CdS catalyst loaded with 10 wt % Pt nanocrystals during six-time reaction under visible light irradiation ($\lambda > 420$ nm). Each reaction has been performed for 12 h, and the generated hydrogen was collected by displacing the water in graduated cylinder. The rate of hydrogen production, which was initially equal to 4.1 mmol h^{-1}, slowly decreased and stably maintained at 1.6 mmol h^{-1} after six-time irradiation.

In order to determine whether the regression of activity observed was linked only to the decreasing concentration of SO_3^{2-} and S^{2-} ions or whether it was due to an effective deactivation of the photocatalyst, the CdS suspension was filtered and subsequently redispersed in the fresh reaction solution during the second illumination period. The initial rate of hydrogen evolution is 3.5 mmol h^{-1}, instead of 4.1 mmol h^{-1}, which indicates a deactivation equal to 15% for the first run of reaction. The deactivation of the photocatalyst may be due to several processes; the contamination of the platinum reduced at the CdS surface by sulfurous products to form platinum sulfide, as is usually the case on Pt catalyst, is perhaps the most important. Further, an increasing concentration of the oxidation state of sacrificial regents also suppresses the proceeding of photocatalytic reaction.

3.3. Role of Sacrificial Reagents. The efficient photocatalytic hydrogen production using sunlight requires sufficiently negative flat-band potential and good absorption properties in the visible for semiconductor photocatalysts. CdS has a good absorption up to 520 nm and a flat-band potential at −0.66 V (pH 7), which is a very promising photocatalyst. Although CdS is not stable in aqueous solutions under irradiation due to the anodic dissolution, such a disadvantage can be avoided in the presence of sacrificial reagents of S^{2-} and SO_3^{2-}. We analyzed the chemical composition of reaction solution after the photocatalytic reaction shown in Figure 6d, and the ions of $S_2O_3^{2-}$, SO_4^{2-}, and S_2^{2-} were examined. The reaction mechanism for the photocatalytic hydrogen production over CdS in the presence of S^{2-} and SO_3^{2-} is similar to previous results.[24,33]

When a photon is absorbed by CdS in the presence of S^{2-} and SO_3^{2-}, an e^-/h^+ pair is generated, as described by eq 1.

charge carrier generation:

$$CdS + h\nu \xrightarrow{h\nu > 420\ \text{nm}} h^+ + e^- \quad (1)$$

The e^- and h^+ may migrate to the surface and react with the adsorbed reactants in the desired process, or they may undergo undesired recombination. A rate increase in the former process or a rate decrease in the latter would lead to greater photocatalytic efficiency. The photogenerated electrons in the conductive band reduce the water to form hydrogen, as described by eq 2.

charge carrier trapping for the formation of hydrogen:

$$2e^- + 2H_2O \rightarrow H_2 + 2OH^- \quad (2)$$

Meanwhile, the photogenerated holes in the valence band oxidize SO_3^{2-} and S^{2-} to form SO_4^{2-} and S_2^{2-} directly, according to eqs 3 and 4, respectively.

The oxidation of sulfite with the concomitant formation of hydrogen follows two different routes forming sulfate and disulfide ions in alkaline aqueous solution:

$$SO_3^{2-} + 2OH^- + 2h^+ \rightarrow SO_4^{2-} + 2H^+ \quad (3)$$

$$2S^{2-} + 2h^+ \rightarrow S_2^{2-} \quad (4)$$

The production of S_2^{2-} ions, which act as an optical filter and compete with the reduction of protons, was efficiently suppressed by mixing with SO_3^{2-} ions, according to eq 5. SO_3^{2-} ions yields mainly thiosulfate ions:

$$S_2^{2-} + SO_3^{2-} \rightarrow S_2O_3^{2-} + S^{2-} \quad (5)$$

The presence of excess S^{2-} ions in the reaction solution also stabilizes the photocatalyst surface because the formation of sulfur defects could be suppressed. The buildup of disulfide ions is extensively suppressed by the addition of SO_3^{2-} ions. Compared with the yellow disulfides, the anodic reaction product thiosulfate is colorless and thus does not reduce the light absorption of CdS. Furthermore, thiosulfate ions do not interfere significantly with protons in the reduction process. However, the hydrogen formation can drop due to the excess consumption of SO_3^{2-} and S^{2-} ions present through eq 6:

$$SO_3^{2-} + S^{2-} + 2h^+ \rightarrow S_2O_3^{2-} \quad (6)$$

From above, hydrogen produced by irradiating suspensions of platinized CdS in electrolyte solutions of S^{2-} and SO_3^{2-} can show very high efficiency.

3.4. Role of Structure of CdS Photocatalyst. CdS is a well-known n-type semiconductor photocatalyst with very suitable band structure and band gap for visible-light-driven photocatalytic hydrogen production. However, it is not easy to prepare very active CdS because many factors, such as preparation conditions, shape, size, crystallinity, and so on, can influence the photocatalytic activity of CdS. In order to design highly active CdS photocatalyst, three strategies need to be considered. First, monodisperse Pt nanocrystals on the surface of CdS are necessary. It is known from luminescence quenching experiment that S^{2-} ions are very efficient hole acceptors, therefore allowing a good separation of charge carriers. Although the intense cathodic flat-band

shift obtained with S^{2-} ions allows hydrogen to be produced in the absence of an electron transfer catalyst like platinum, the loading of monodisperse Pt nanocrystals on the surface of CdS can greatly improve the photoctalytic efficiency because the surface Pt−CdS nanostructure changes the Fermi level equilibration and band structure of CdS through storing and shuttling photogenerated electrons from the CdS to acceptors in a photocatalytic process. Second, CdS needs a large surface area. Because of the weaker interaction of SO_3^{2-} ions with the CdS surface, the hole transfer is less efficient, and thus the probability of e^-/h^+ recombination is higher. Elimination of the surface recombination is an essential condition for obtaining redox with the SO_3^{2-} electrolyte. One way to solve this problem is to prepare CdS with large surface area for increasing the CdS−electrolyte interface area, which has been solved in the present study by creating nanopores within CdS nanostructures. Third, the e^-/h^+ pairs generated in the body of CdS separate, migrate to the surface of CdS, and react with the adsorbed reactants, which greatly improves the photocatalytic efficiency when compared with the reaction solely involving the electrons and holes photogenerated on the surface. It was known that sulfides with small surface areas of $<10\ m^2\ g^{-1}$ still showed good photocatalytic efficiency because of their good crystallinity and less crystal defects that can largely reduce the bulk electron–hole recombination during the migration of electrons and holes to the surface of CdS. Although the crystal defects can be decreased through long-time solid-state reaction or calcination at high temperature, the crystal defects are inevitable, and a small surface area cannot give very fast interfacial charge carrier transfer. Therefore, to design nanoporous CdS with special hollow and sheetlike nanostructures that can shorten the bulk-to-surface migrating distance of electrons and holes can thoroughly improve the photocataytic activity of CdS.

3.5. Strategy for Prepare Crystalline Nanoporous CdS Nanostructures. In order to prepare crystalline nanoporous CdS nanostructures, we proposed a two-step aqueous solution synthesis strategy. CdS nanocrystals have been synthesized by the solution methods such as aqueous precipitation from inorganic reactants of Cd^{2+} and S^{2-}, thermolysis of organic complexes precursors in solvents, and hydrothermal/solvothermal reaction[59–61] The solubility product (K_{sp}) for CdS is very small, which results in a fast nucleation of fine CdS nanocrystals suffering from disadvantages of particles agglomeration. Although monodisperse CdS nanocrystals can be obtained by using surfactant coating, the obtained CdS nanocrystals only dispersed in nonpolar solvents.[62] Some high-temperature synthesis methods such as CVD, etc.,[63] have been used to prepare CdS nanomaterials; however, the obtained CdS are nanoporous, connected, and with relatively large size.

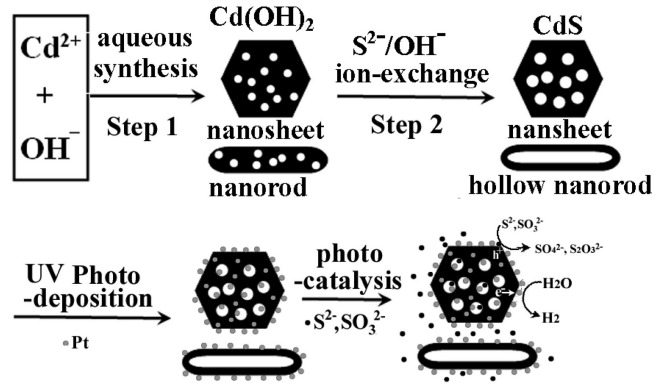

Figure 7. A schematic representative of the synthesis route, photodeposition of monodisperse Pt nanocrystals, and photocatalytic hydrogen production in the presence of SO_3^{2-} and S^{2-} over nanoporous CdS nanostructures of nanosheets and hollow nanorods.

In comparison to CdS, $Cd(OH)_2$ can be prepared by simple aqueous precipitation of Cd^{2+} in basic solution, and the size of synthesized $Cd(OH)_2$ can be controlled in relatively large size because of its relatively large solubility product constant (K_{sp}) that varies by changing pH value of solution, and thus the nucleation rate of $Cd(OH)_2$ can be controlled at a relatively slow rate, which results in the formation of size-controlled $Cd(OH)_2$. Further, the K_{sp} of CdS is far larger than that of $Cd(OH)_2$, and thus CdS can be synthesized from $Cd(OH)_2$ by S^{2+}/OH^- ion-exchange reaction which will process from the outer surface into the inside of the $Cd(OH)_2$. Because the lattice cell parameters of a and c of hexagonal CdS respectively are 4.140 and 6.719 Å, which are larger than the cell parameters of $a = 3.493$ Å and $c = 4.710$ Å for $Cd(OH)_2$. Meanwhile, the density of CdS is 4.65 g/cm^3, which is smaller than 4.79 g/cm^3 for $Cd(OH)_2$. The volume expansion results in the formation of either CdS nanosheets containing much larger nanopores from nanoporous $Cd(OH)_2$ nanosheets or hollow CdS nanorods from solid $Cd(OH)_2$ nanorods.

On the basis of the above analysis, a schematic description for the synthesis, photodeposition of Pt nanocrystals, and photocatalytic reaction is shown in Figure 5. The obtained CdS exhibited the highest apparent quantum yield of about 60.34% for hydrogen production under visible light at 420 nm, indicating the potential for very practical photocatalytic hydrogen production with sunlight. The nanoporous and hollow nanostructures are very important for the present CdS photocatalysts with high photocatalytic activity, which can be applied for designing other highly active photocatalysts. The present synthesis strategy could be a general method for other nonporous hollow nanostructures of binary sulfides because solubility product constant (K_{sp}) of most metal hydroxides is larger than that of corresponding metal sulfides.

Acknowledgment. We thank the Japan Society for the Promotion of Science (JSPS) Fellowship, Research Grant-in-Aids of the Ministry of Education, Culture, Sports, Science and Technology of Japan (MEXT), the New Energy and Industrial Development Organization (NEDO), and the Solution Oriented Research for Science and Technology (SORST) program of the Japan Science and Technology (JST) Corporation. The authors are grateful to reviewers for their helpful suggestions and comments.

CM7029344

(59) So, W.; Jang, J. S.; Rhee, Y. W.; Kim, K. J.; Moon, S. J. *J. Colloid Interface Sci.* **2001**, *237*, 136.
(60) Li, Y. D.; Liao, H.; Ding, Y.; Fan, Y.; Zhang, Y.; Qian, Y. *Inorg. Chem.* **1999**, *38*, 1382.
(61) Nair, P. S.; Radhakrishnan, T.; Revaprasadu, N.; Kolawole, G. A.; O'Brien, P. *Chem. Commun.* **2002**, 564.
(62) Joo, J.; Na, H. B.; Yu, T.; Yu, J. H.; Kim, Y. W.; Wu, F.; Zhang, J. Z.; Hyeon, T. *J. Am. Chem. Soc.* **2003**, *125*, 11100.
(63) Ge, J.; Li, Y. D. *Adv. Funct. Mater.* **2004**, *14*, 157.